IRANIAN JOURNAL OF CATALYSIS

Study of catalytic performance of $LaMnO_3$ and $LaMnO_3$-ZSM-5 nanocatalysts toward 2-propanol conversion

Seyed Ali Hosseini*

Department of Applied Chemistry, University of Urmia, Urmia, Iran.

Received 4 April 2015; received in revised form 21 September 2015; accepted 27 September 2015

ABSTRACT

$LaMnO_3$ and $LaMnO_3$/ZSM-5 nano catalysts were synthesized by Pechini method and their physical-chemical properties were characterized using XRD, FTIR, SEM-EDX, UV-vis DRS, BET surface area and TPR. The correlation between characteristic properties and activity of catalysts were investigated. The catalytic performance of the catalysts was evaluated in combustion of 2-propanol and compared with 1% Pt/Al_2O_3 performance. The results of SEM and UV-Vis DRS of $LaMnO_3$/ZSM-5 indicated the well dispersion of the perovskite oxide on the support. The results of TPR indicated no direct correlation between the activity and reducibility of the catalysts. The catalytic studies revealed that the supporting of $LaMnO_3$ increased the conversion rate of 2-propanol, which is ascribed to higher surface area, more availability of catalytic sites to probe molecules. In addition, the stability of $LaMnO_3$/ZSM-5 was higher than that of $LaMnO_3$ during a 10 h time on stream. The conversion rate of 2-propanol on the $LaMnO_3$/ZSM-5 was higher even than that on the industrial $1\%Pt/Al_2O_3$ catalyst. The study showed that the perovskite/zeolite catalyst could be promising catalysts in the removal of VOCs.

Keywords: *Nano perovskite, Conversion rate, Catalytic combustion, UV-Vis DRS, 2-Propanol.*

1. Introduction

One of major challenges of human in 21th century is environmental pollution. Volatile organic compounds (VOCs), having a vapor pressure larger than 13.3 Pa at 25°C, are an issue of major concern for many scientists worldwide because of their contribution to major environmental problems such as, photochemical smog formation, global warming, stratospheric ozone decrease and odor nuisance [1,2]. From economical point of view, catalytic remediation is a widely used technology to control the emissions of volatile organic compounds (VOCs) [3]. In this process many types of catalysts have been evaluated. Metal mixed oxides are of promising catalysts from view point of cheapness and abundance [4,5]. Improved properties of mixed oxides against simple ones are well known, especially in the environmental protection field. Among mixed oxides, perovskites are thermal stable and show the high catalytic activity for complete oxidation of hydrocarbons and NO_x removal.

*Corresponding author email: s_ali_hosseini@yahoo.com
Tel.: +98 44 3275 5294; Fax: +98 44 3275 5294

Perovskite oxides are usually represented by the ABO_3 general formula where A is lanthanide and/or alkaline earth metal ion and B is a transition metal ion. In these materials, the nature of cations in B site, determines the catalytic activity of oxide [6].

Among perovskite, lanthanum manganite exhibit promising activity in catalytic oxidation [7,8]. These oxides have been extensively studied because of the possibility that they can be substituted for precious metal catalysts in many reactions [9,10]. So far, two kinds of processes have been mainly used for the preparation of perovskite oxides. The one is the solid-state reaction process and the other includes chemical solution processes (wet processing). The former process needs high calcination temperatures usually higher than 1000°C for the preparation of perovskite oxides, which gives rise to the formation of oxides with low surface areas and large particle sizes [11]. Therefore, much attention has been focused on the chemical solution processes including co-precipitation, sol–gel, and complexing methods to obtain perovskite oxides with high surface areas [12-16]. These methods were effective in obtaining perovskite nano-particles at lower calcination temperatures.

In some cases, however, the processes are complicated and a large quantity of organic solvents is necessary. However, the major limitation of these results is their lower surface area and their increased tendency to sinter. In this view, the only solution of increasing the contact surface between the VOC and the perovskite is to disperse it on a large surface area and thermally stable support and using of novel synthesis method to get nanoparticle size.

Two problems arise when supporting an active phase: the preservation of the structure or accepting/ generating a controlled alteration and a good and uniform dispersion. Zeolites are of acid type supports which are used in catalytic reactions. They are crystalline alumino-silicates with cavities, whose sizes can vary in the range from one to several tens of nanometers.

ZSM-5 zeolite is a synthetic high specific surface area which is used as catalyst and support in industry. The ratio of Si/Al in zeolite structure is an influencing factor on catalytic activity of catalyst [17]. $LaMnO_3$ is one of high active perovskite in environmental protection [6]. $LaMnO_3$ was chosen as a model of perovskite catalyst. To our knowledge, the catalytic performance of $LaMnO_3$ supported on ZSM-5 zeolite has not been studied in catalytic oxidation of volatile organic compounds.

So, the objectives of this work were to study the catalytic activity of $LaMnO_3$ and $LaMnO_3$-ZSM-5 obtained from the pechini type sol gel in combustion of 2-propanol and compare their activity to that of 1% Pt/Al_2O_3. The activity of catalysts was calculated base of the conversion rate of 2-propanol over active sites of the catalysts. The activity of catalysts was tested in catalytic combustion of 2-propanol as a model of oxygenated volatile organic compound. The catalysts were characterized by XRD, FTIR, SEM-EDX, UV-Vis, BET surface area and TPR.

2. Experimental

2.1. Catalyst preparation

$La(NO_3)_3$. $6H_2O$, $Mn(NO_3)_2$. $4H_2O$, and citric acid monohydrate as starting materials were prepared from Merck Company. ZSM-5 zeolite with Si/Al ratio of 14 was obtained from ZeoChem, Swiss. Perovskite was prepared by pechini type sol gel method, described elsewhere [18-19].

Briefly, aqueous solution of La and Mn nitrates with cation ratios 1:1 was mixed for 30 minutes at 60˚C and then citric acid and ethylene glycol were used as the monomers for the formation of the polymeric matrix. Proper amounts of citric acid and ethylene glycol (molar ratio = 1:4) were added to a mixture of stock solutions of metal nitrates. Three major reactions: chelation, esterification, and polymerization successively occurred and black polymeric precursor formed.

The solution was left to evaporate the extra water at 80˚C with continuous mechanical stirring, until a sticky gel was obtained. In order to carry out the gel decomposition under controlled conditions, the temperature was gradually raised to 200 ˚C and finally the decomposed gel self-ignited. The spontaneous combustion lasted for 10–20 s and gave rise to the powdered product. The combusted powders were then fired in static air at 700 ˚C for 6 h.

The synthesis of $LaMnO_3$/ZSM-5 was similar to that of $LaMnO_3$, just ZSM-5 was added after addition of ethylene glycol and other step continued the same. The mass ratio of $LaMnO_3$ to ZSM-5 was 2:1.

2.2. Catalyst characterization

For FT-IR spectroscopy, the samples were pressed into self-supporting wafers of 10-15 mg/cm^2 surface density and placed into a glass cell sealed by KBr windows. The spectra were recorded in transmittance at room temperature using a Bruker spectrometer (model TENSOR 27).

X-ray diffraction was used to identify the crystalline phases identification using a SIEMENS D500 diffractometer and Cu Kα radiation (λ = 1.54 ˚A). Diffractograms were recorded with a step of 4˚ per minute for 2θ between 15 and 75˚. Phase recognition was made by comparison with JCPDS files. Particle sizes (D) were evaluated by means of the Scherrer equation $D = K\lambda/(\beta \cos \theta)$. K is a constant equal to 0.89. λ is the wavelength of the X-ray and β is the effective line width of the X-ray reflection. The BET surface area and pore volume of samples were determined from N_2 isotherms measured at -196˚C using a micro pore analyzer (ASAP 2010, USA).

Temperature programmed reduction (TPR) measurements were carried out with Micrometrics Autochem 2900. Samples were pre-treated with a gaseous mixture containing 5 vol % oxygen in helium at 500˚C for 2 h. Hydrogen consumption was measured with a mixture of 5 vol % H_2 in argon at 20 cm^3. min^{-1} and a linear heating rate of 10 ˚C/min at 50-950˚C.

The morphology of the mixed oxides was determined via scanning electron microscopy (SEM) by EQ-C1-1 instrument, equipped with X-ray energy dispersive spectroscopy (EDS) analyzers.

The nature and coordination of cations in the samples were determined by recording UV-Vis diffuse reflectance spectra of samples in the wavelength range

of 300-1000 nm, using a Scinco210 spectrophotometer (model AA-1301) equipped with an integral sphere.

2.3. Catalytic Studies

The catalytic activity of catalyst was tested in a laboratory setup, described in our previous papers [4-6]. The combustions of organic compound were carried out in a straight quartz reactor (l=60 cm, i.d.= 0.8 cm) at different temperatures under atmospheric pressure. The catalyst (200 mg) inserted between two quartz wool plugs. A K-type thermocouple used to control the temperature.

Before reaction tests, the catalysts were pretreated with air (40 cm^3/min) at 300 ˚C for 2h. Total flow rate of feed was 100 $cm^3.min^{-1}$. The VOC-laden stream was generated at a fixed concentration by bubbling nitrogen gas inside VOC saturator. The flow of gases was controlled by a needle valve (Parker Company, USA). Nitrogen was carrier gas, and using a calibrated soap bubble flow meter the volume flow rates were measured. The concentration of VOCs in the gaseous feed was 0.2% mol/mol. The hourly gas flow space velocity (GHSV) was around 5000 h^{-1}, and the reaction temperature ranged from 120-400 ˚C. The catalytic reactions were operated under steady state in which all process variables remained constant with time at any given point in the reactor before any measurement was made. The feed and product gases were analyzed using an off-line Shimadzu 2010 gas chromatograph (GC) equipped with a FID detector and a CBP20 column (l = 25 m, i.d. = 0.25 mm). Helium was used as carrier gas.

3. Results and Discussion

In the synthesis of samples, the mole ratio of citrate/nitrate as fuel/oxidant was kept 0.4, the ratio recommended by Deganello [20] and co-worker for synthesis of perovskites and used in our previous work [6]. The XRD patterns of the catalysts are shown in Fig. 1. $LaMnO_3$ catalysts are single phase perovskite oxides, with primitive rhombohedral cell, R.3m space group as compared with literature (JCPDS: 35-1353) [21].

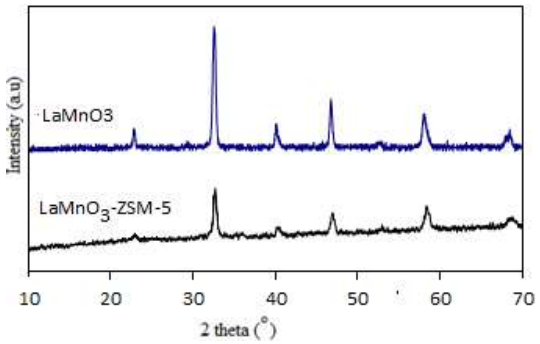

Fig. 1. X-ray patterns of $LaMnO_3$ and $LaMnO_3$-ZSM-5.

Generally, the XRD pattern of $LaMnO_3$ and $LaMnO_3$-ZSM-5 looks similar, but the intensity of peaks at the pattern of $LaMnO_3$-ZSM-5 is lower than that of $LaMnO_3$. It is attributed to the presence of support in the matrix of support decreased the crystallinity of the sample and thus the intensity of peaks decreased in the supported manganites. In addition, the peaks of $LaMnO_3$-ZSM-5 have shifted a little bit to higher 2theta. The mean crystallite sizes of oxides were estimated from the full width at half-maximum of the most intense and non-overlapped diffraction (~2θ=32.6°), using Debye Scherrer equation.

The mean crystalline domain size obtained for $LaMnO_3$ and $LaMnO_3$-ZSM-5 was 38 and 24.5 nm, respectively. XRD results indicated that the crystallites of $LaMnO_3$-ZSM-5 are smaller than those of $LaMnO_3$. The XRD results indicated that pechini method is a successful in forming a perovskite phase with a higher degree of crystallinity.

The formation of perovskite structure in the samples was confirmed by FT-IR spectroscopy (Fig. 2). In FT-IR spectra of $LaMnO_3$: the broad band at 3410 cm^{-1} is attributed to the presence of co-ordinate/entrapped water, which is rapidly absorbed by KBr [7]. The bands around 594 and 486 cm^{-1} are attributed to the Mn–O stretching vibration (ν_1 mode) and the O–Mn–O deformation vibration (ν_2 mode), respectively. In the case of FT-IR of $LaMnO_3$–ZSM-5, except two above bands, the bands at 440, 741, and 1060 cm^{-1} are attributed to the vibrational modes of ZSM-5 zeolite [22-23]. The 1060 cm^{-1} band is due to the asymmetric stretching vibration modes of internal T-O bonds in TO_4 (T=Al or Si) tetrahedral. The 440 and 741 cm^{-1} are assigned to the stretching vibration modes of O-T-O groups and the bending vibration modes of T-O bonds, respectively.

The morphology and particle size of perovskite samples are investigated by scanning electron microscopy. The SEM images and energy dispersive x-ray (EDX) spectra of samples are shown in Fig. 3.

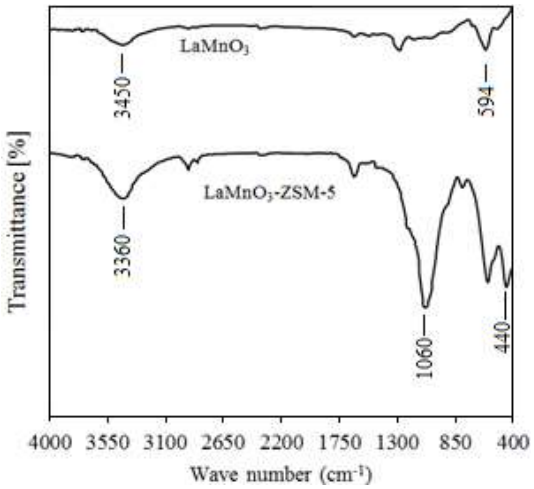

Fig. 2. FTIR spectra of $LaMnO_3$ and $LaMnO_3$-ZSM-5.

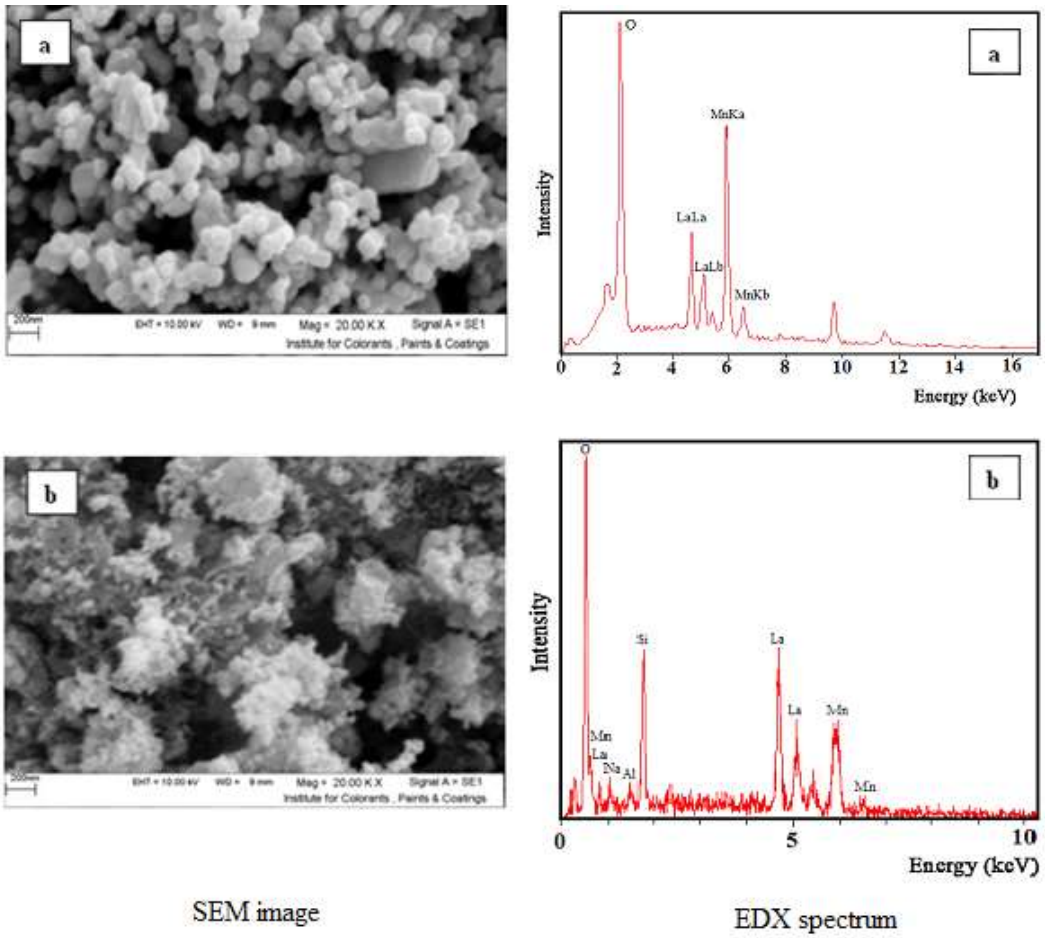

Fig. 3. SEM micrographs and EDX analysis of $LaMnO_3$ (a) and $LaMnO_3$-ZSM-5 (b).

Fig. 3a shows the SEM image and the EDX spectrum of $LaMnO_3$ powder. As shown, the particles are uniform in the range 60-90 nm. However, some large particle/agglomeration is observed in Fig. 3a. The EDX spectrum of $LaMnO_3$ shows the relative abundance of the constituent elements of the sample, which the results of relative analysis as number are presented in Table 1. Fig. 3b shows the SEM image and the EDX spectrum of $LaMnO_3$-ZSM-5. The SEM image indicates that $LaMnO_3$ particles are well-supported on ZSM-5 particles. Considering the sizes of crystallites and particles, it can be concluded the $LaMnO_3$ particles contain low crystallites. The EDX spectrum show the elemental analysis of the sample and the relative abundance of the elements in the samples are presented in Table 1. It is concluded that most of the surface of the sample are covered by $LaMnO_3$.

The TPR curve of $LaMnO_3$ and $LaMnO_3$-ZSM-5 samples calcined at 700°C is presented in Fig. 4.

Table 1. Results of EDX analysis.

Element	$LaMnO_3$-ZSM-5		$LaMnO_3$	
	W%	A%	W%	A%
O	10.16	37.37	12.02	42.01
Na	1.54	3.93	0	0
Al	1.02	2.23	0	0
Si	1.29	2.70	0	0
Mn	26.78	28.68	27.52	30.47
La	59.21	25.08	60.46	27.52
	100.00	100.00	100	100

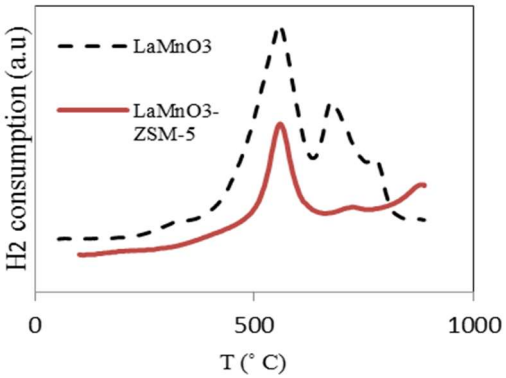

Fig. 4. TPR curves of the catalysts.

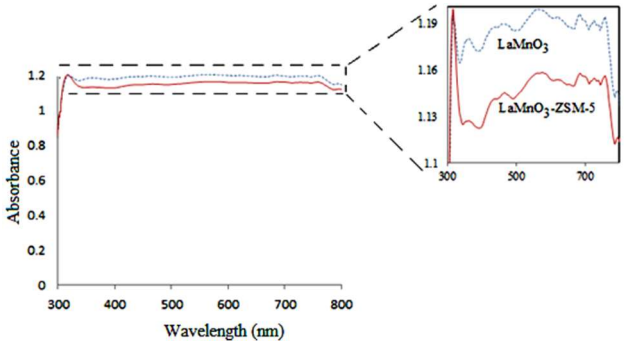

Fig. 5. UV-Vis DRS spectra of the catalysts.

The reduction profile is characterized by two temperature regions. The reduction profiles of catalysts in the low temperature region are similar. In the low temperature region around 309°C the reduction of Mn^{4+} to Mn^{3+} ions and removal of oxygen from the perovskite structure and the reduction peak around 548°C is ascribed to reduction of Mn^{3+} to Mn^{2+} ions in the perovskite structure.

In the case of $LaMnO_3$–ZSM-5, the reduction peaks of perovskite shift to higher temperatures. This is attributed to this fact that the Si/Al affects the reducibility of $LaMnO_3$ in supported catalysts. Even, it is well-known that the reducibility is controlled by the local Si/Al ratio in the zeolite, then influencing their reducibility [24].

DRS is a useful method to obtain information on surface coordination and different oxidation states of metal ions by measuring d–d, f–d transitions and oxygen–metal ion charge transfer bands. In this work, UV–vis spectra were recorded for the samples in order to understand the nature and coordination of manganese cations in the samples. The UV–vis spectra of samples are shown in Fig. 5. In the range 210-342 nm, absorption bands are observed for all samples. The intensity of the band at around 316 nm in the samples is indicative of the presence of well dispersed crystalline Mn_2O_3 species on the surface [11]. As observed in Fig. 5, the higher intensity of this band for $LaMnO_3$-ZSM-5 may indicate the greater development of small crystallites of Mn_2O_3, in accordance with XRD results.

Table 2. Specific surface area and pore volume of the samples.

Catalyst	Multipoint BET surface area	BJH surface area	Pore volume (cc/g)
$LaMnO_3$	16.8	15.7	0.146
$LaMnO_3$-ZSM-5	100.3	98.6	0.412
1% Pt/Al_2O_3	133	129	0.493

Fig. 6 shows the N_2 adsorption isotherms of the samples. Table 2 presents the multipoint BET surface area, BJH method cumulative adsorption surface area, and pore volume of the samples. The multi-point BET surface area of $LaMnO_3$, $LaMnO_3$-ZSM-5 and 1% Pt/Al_2O_3 is 16.8, 100.3 and 133 m^2/g, respectively. Regards to the specific surface area of ZSM-5 (310 m^2/g), it is resulted that the introducing of $LaMnO_3$ significantly decreased the surface of $LaMnO_3$-ZSM-5.

The catalytic activity of catalysts was evaluated in gas phase catalytic combustion of 2-propanol (Fig. 7). $T_{50\%}$ is a criterion for comparison of the conversion rate of reactant over the catalyst. The ignition temperature $T_{50\%}$, defined as the temperature required to reach 50% conversion for 2-propanol, is shown in Table 3. The $T_{50\%}$ was lowered by 9˚C on $LaMnO_3$-ZSM-5 comparison with $LaMnO_3$. Considering both the reaction temperature and the conversion (Table 3, Fig. 7), it is resulted that the activity of $LaMnO_3$-ZSM-5 is higher than that of $LaMnO_3$ and 1% Pt/Al_2O_3 under the same conditions during the total combustion of 2-propanol. Three factors chiefly affect the catalytic activity of the perovskite catalysts: chemical composition, degree of crystallinity and the crystal morphology (including specific surface area, particle size and pore distribution of the perovskite catalysts). Considering the XRD patterns of samples indicated a higher degree of crystallinity in samples. Comparison the results of the activity and BET results indicate a direct relationship between activity and surface area of the catalysts. As a result, it can be concluded that the specific surface area plays a more important role than other studied factors. Despite this, it is not concluded any direct relationship between reducibility and the activity of the catalysts.

Table 3. $T_{50\%}$ of 2-propanol over different catalysts.

Catalyst	$T_{50\%}$(˚C)
$LaMnO_3$	178
$LaMnO_3$-ZSM-5	169
1% Pt/Al_2O_3	226

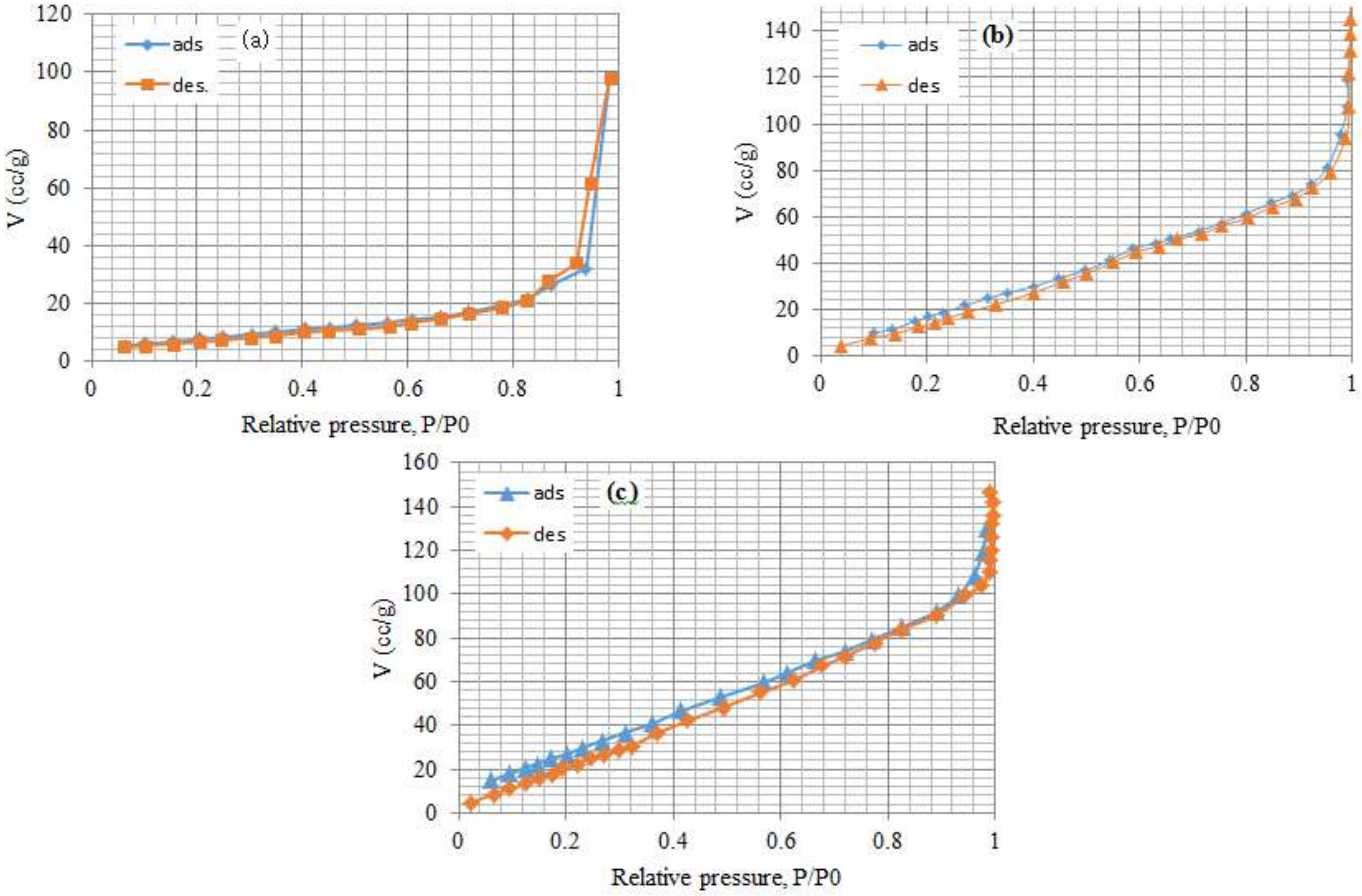

Fig. 6. N_2 adsorption Isotherm of the samples; $LaMnO_3$ (a), $LaMnO_3$ –ZSM-5 (b), 1% Pt/Al_2O_3 (c).

In order to study the activity of catalyst in more precision and more details, we calculated the rate of 2-propanol conversion per gram of the perovskite and Pt. The results are presented in Table 3. It should be noted that in order to use the rate equation of differential reactors (Eq. 1), the conversion should be less than 0.2 and so the conversion at temperature 120˚C was considered.

$$r_a = F_A X_A / W_{cat} \qquad \text{(Eq. 1)}$$

Where r_a is specific rate of catalytic reaction, F_A is the molar flow rate (mol/s), X_A is the 2-propanol conversion and W_{cat} is the weight of catalyst by gram. It is observed in the Table that the rate of 2-proponal conversion on $LaMnO_3$-ZSM-5 is higher than $LaMnO_3$. According the results reported in literature, supporting on larger surface area supports increases the surface area of active catalyst and decreases the $T_{50\%}$. Based on the BET and SEM results, it is concluded that particles of perovskite in $LaMnO_3$–ZSM-5 are well-dispersed on the ZSM-5 zeolite and so 2-propanol molecules can easily react on their surface. This justifies the higher activity of $LaMnO_3$–ZSM-5 compared to $LaMnO_3$. Two values for rate of 2-propanol are reported in Table 3. First one is the calculation based on the weight of perovskite in the catalyst, i.e. 22.12×10^{-7} and the second is based on total weight of the catalyst, i.e. 7.3×10^{-7} mol. s^{-1}. g_{cat}^{-1}.

In addition, the activity of $LaMnO_3$–ZSM-5 catalyst was compared with that of an industrial catalyst, i.e. 1% Pt/Al_2O_3. According to the conversion, the conversion of 2-propanol was 0.19 and 0.10 over $LaMnO_3$–ZSM-5 and 1% Pt/Al_2O_3, respectively. The conversion rate of 2-propanol on $LaMnO_3$–ZSM-5 is higher than that over 1% Pt/Al_2O_3 based on the total mass of catalyst (Table 4).

Table 4. Conversion rate of 2-proponal conversion over different catalysts.

Catalyst	Conversion	r_a (mol. min^{-1}. g_{cat}^{-1}) based on weight of loaded catalyst	r_a (mol. min^{-1}. g_{cat}^{-1}) based on total weight of the catalyst
$LaMnO_3$	0.16	5.92×10^{-7}	5.92×10^{-7}
$LaMnO_3$-ZSM-5	0.19	22.12×10^{-7}	7.3×10^{-7}
%Pt/Al_2O_3	0.10	3.7×10^{-5}	3.7×10^{-7}

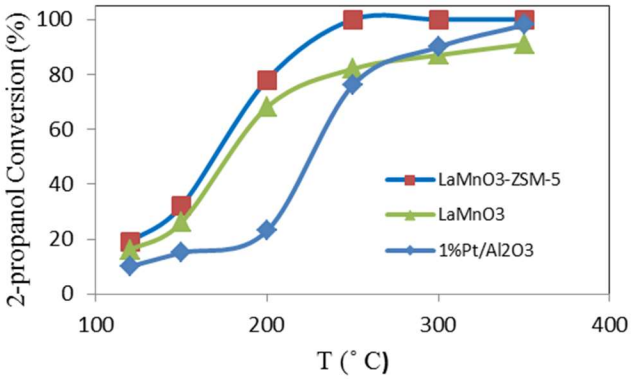

Fig. 7. Light-off curves for catalytic combustion of 2-propanol.

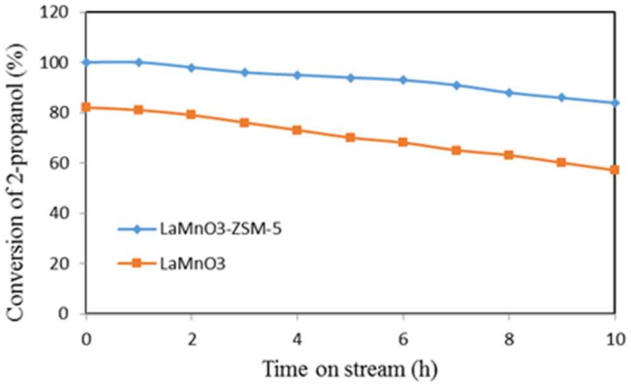

Fig. 8. Conversion vs. time on-stream curves for 2-propanol combustion on different spinel catalysts.

But if the conversion rate over Pt sites is calculated the conversion rate is 3.7×10^{-5} mol. s^{-1}. g_{cat}^{-1}. However, the ZSM-5 and Al_2O_3 supports could be catalytically active. The conversion rate of 2-propanol over perovskite phase is lower than Pt, but it is higher than most other catalysts in the catalytic combustion of 2-propanol, which are presented in Table 5 [6,25,26]. In this table, $T_{50\%}$, the temperature for the conversion of fifty percent of 2-propanol was considered as a criteria of catalyst activity. It is observed that $T_{50\%}$ for conversion of 2-propanol on $LaMnO_3$ and $LaMnO_3$-ZSM-5 is lower than that on the other catalysts, indicating that these catalysts are more active. T50% of 2-propanol conversion on $LaMnO_3$-ZSM-5 is the lowest among the catalyst series in Table 5, hence it is considered as the most active catalyst. $LaMnO_3$-ZSM-5 exhibited higher activity not only than $LaMnO_3$, but also it was more active than gold catalysts i.e. Au/Al_2O_3, $Au/10CeO_2/Al_2O_3$, and $Au/1.5CeO_2/Al_2O_3$ for oxidation of 2-propanol [26].

The used catalysts were treated by heating at 400 ˚C under passing air for 1h. The treated catalysts were reused in catalytic oxidation of 2-propanol. No considerable decrease in the activity of the treated catalysts was observed. After three times of catalyst usage, approximately 2 % decrease in conversion of 2-propanol was resulted.

In addition to the activity tests, some additional experiments were conducted to examine the stability of catalysts in the combustion of 2-propanol at a reaction temperature of 250˚C. The profiles of 2-propanol conversion for periods on-stream of 10 h are displayed in Fig. 8. From the data collected in Fig. 8, it is obvious that after 10 h, the conversion of 2-propanol over $LaMnO_3$-ZSM-5 catalysts reached ca. 84%, whereas in the case of $LaMnO_3$ activity dropped to ca. 57%. It is resulted that the rate of deactivation of $LaMnO_3$-ZSM-5 is slower than that of $LaMnO_3$.

4. Conclusions

The correlation between rate of 2-propanol conversion and physical-chemical properties of $LaMnO_3$ and $LaMnO_3$-ZSM-5 was studied. The XRD results revealed that the pechini method is a promising method for synthesis of high crystalline perovskite nano oxides. The results of SEM and UV-Vis DRS revealed the good dispersion of $LaMnO_3$ particles on the zeolite support.

Table 5. $T_{50\%}$ for conversion of 50% of 2-propanol.

Catalyst name	$T_{50\%}$ for 50% conversion of 2-propanol
$CoMn_2O_4$ [25]	222
$CoCr_2O_4$ [5]	225
$LaCoO_3$	228
$LaMnO_3$	177
$LaMnO_3$-ZSM-5	170
Au/Al_2O_3 [26]	300
$Au\text{-}1.5CeO_2/Al_2O_3$ [26]	262
$Au\text{-}10CeO_2/Al_2O_3$ [26]	212

No direct relationship was concluded between activity and reducibility of the catalysts. The higher activity of supported lanthanum manganite is attributed to the higher surface area of catalyst, small particles of $LaMnO_3$ and subsequently the 2-propanol molecules can easily access to active sites of catalyst and react with oxygen. $LaMnO_3$-ZSM-5 showed higher activity, even than 1% Pt/Al_2O_3. The study revealed that the supporting of the perovskite-type catalyst on the zeolites improved the activity of the catalyst. $LaMnO_3$-ZSM-5 exhibited the higher activity and stability than $LaMnO_3$ in catalytic combustion of 2-propanol revealing the superior role of ZSM-5 support in improving the activity of the catalyst. $LaMnO_3$-ZSM-5 could be a promising catalyst in environmental control applications.

Acknowledgements

The author is thankful to those, who contributed to enhance this project especially Iranian Nanotechnology Initiative for their encouragement support.

References

[1] S. Arefi-Oskoui, A. Niaei, H.H. Tseng, D. Salari, B. Izadkhah, S.A. Hosseini, ACS Comb. Sci. 15 (2013) 609−621.
[2] S.A. Hosseini, M. Sadeghi, A. Alemi, A. Niaei, D. Salari, L. Kafi Ahmadi, Chin. J. Catal. 31 (2010) 747-750.
[3] S.A. Hosseini, M. Sadeghi, L. Kafi Ahmadi, A. Alemi, A. Niaei, D. Salari, Chin. J. Catal. 32 (2011) 1465-1468.
[4] S.A. Hosseini, A. Niaei, D. Salari, M.C. Alvarez-Galvan, J.L.G Fierro, Ceram. Int. 40 (2014) 6157–6163.
[5] S.A. Hosseini, M.C.Alvarez-Galvan, J.L.G.Fierro, A. Niaei, D. Salari, Ceram. Int. 39 (2013) 9253–9261.
[6] S.A. Hosseini, D. Salari, A. Niaei, S. Arefi Oskoui, J. Ind. Eng. Chem. 19 (2013) 1903–1909.
[7] M.C. Alvarez-Galvan, V.A. Pena O'Shea, G. Arzamendi, B. Pawelec, L.M. Gandia, J.L.G. Fierro, Appl. Catal. B 92 (2009) 445–453.
[8] M. Abdolrahmani, M. Parvari, M. Habibpoor, Chin. J. Catal. 31 (2010) 394–403.
[9] Y. Teraoka, H. Fukuda, S. Kagawa, Chem. Lett. 19 (1990) 1-4.
[10] L.J. Tejuca, J.L.G. Fierro, Properties and Applications of Perovskite-type Oxides, Marcel Dekker, Inc., New York, 1993.
[11] J.B. Smith, T. Norby, Solid State Ionics 177 (2006) 639-646.
[12] H.M. Zhang, Y. Teraoka, N. Yamazoe, Chem. Lett. 16 (1987) 665-668.
[13] Y. Teraoka, H. Kakebayashi, I. Moriguchi, S Kagawa, Chem. Lett. 20 (1991) 673-676.
[14] F.H. Chen, H.S. Koo, T.Y. Tseng, J. Am. Ceram. Soc. 75 (1992) 96-102.
[15] Y. Teraoka, H. Kakebayashi, I. Moriguchi, S. Kagawa, J. Alloys Compd. 193 (1993) 70-72.
[16] R.H.E. Van Doorn, H. Kruidhof, A. Nijmeijer, L. Winnubst, A.J. Burggraaf, J. Mater. Chem. 8 (1998) 2109-2112.
[17] Q. Zhu, X. Zhao, Y. Deng, J. Natur. Gas Chem. 13 (2004) 91-203.
[18] M. Vijayakumar, Y. Inaguma, W Mashiko, Chem. Mater. 16 (2004) 2719-2724.
[19] J. Lin, M. Yu, C. Lin, X. Liu, J. Phys. Chem. C 111 (2007) 5835-5845.
[20] F. Deganello, G. Marcì, G. Deganello, J. Eur. Ceram. Soc. 29 (2009) 439–450.
[21] C. Liang, Y. Lin, Appl Catal. B 107 (2011) 284-293.
[22] I. Othman, R.M. Mohamed, I.A. Ibrahim, M.M. Mohamed, Appl. Catal. A 299 (2006) 95-102
[23] E.M. Flanigen, H. Khatami, H.A. Szymanski, Molecular Sieve Zeolite I, Academic Press, New York, NY, USA, 1971.
[24] M. Alifanti, M. Florea, S. Somacescu, V.I. Parvulescu, Appl. Catal. B 60 (2005) 33-39.
[25] S.A. Hosseini, A. Niaei, D. Salari, S.R. Nabavi, Ceram. Int. 38 (2012) 1655–1661.
[26] P. Lakshmanan, L. Delannoy, C. Louis, N. Biona, J.M. Tatibouët, Catal. Sci. Technol. 3 (2013) 2918–2925.